Available online at www.sciencedirect.com

SCIENCE DIRECT®

Remote Sensing of Environment 93 (2004) 368–380

Remote Sensing of Environment

www.elsevier.com/locate/rse

Quantifying forest above ground carbon content using LiDAR remote sensing

G. Patenaude[a,*], R.A Hill[b], R. Milne[c], D.L.A. Gaveau[d], B.B.J. Briggs[a], T.P. Dawson[a]

[a]*Environmental Change Institute, University of Oxford, 1a Mansfield Road, Oxford, OX1 3SZ, UK*
[b]*Centre for Ecology and Hydrology Monks Wood, Abbots Ripton, Huntingdon, Cambridgeshire, PE28 2LS, UK*
[c]*Centre for Ecology and Hydrology Edinburgh, Bush Estate, Penicuik, Midlothian, EH26 0QB, UK*
[d]*Wildlife Conservation Society-Indonesia Program, Jalan Pangrango No. 8, PO. Box 311, Bogor 16003, West Java, Indonesia*

Received 20 April 2004; received in revised form 17 June 2004; accepted 26 July 2004

Abstract

The UNFCCC and interest in the source of the missing terrestrial carbon sink are prompting research and development into methods for carbon accounting in forest ecosystems. Here we present a canopy height quantile-based approach for quantifying above ground carbon content (AGCC) in a temperate deciduous woodland, by means of a discrete-return, small-footprint airborne LiDAR. Fieldwork was conducted in Monks Wood National Nature Reserve UK to estimate the AGCC of five stands from forest mensuration and allometric relations. In parallel, a digital canopy height model (DCHM) and a digital terrain model (DTM) were derived from elevation measurements obtained by means of an Optech Airborne Laser Terrain Mapper 1210. A quantile-based approach was adopted to select a representative statistic of height distributions per plot. A forestry yield model was selected as a basis to estimate stemwood volume per plot from these heights metrics. Agreement of r=0.74 at the plot level was achieved between ground-based AGCC estimates and those derived from the DCHM. Using a 20×20 m grids superposed to the DCHM, the AGCC was estimated at the stand level and at the woodland level. At the stand level, the agreement between the plot data upscaled in proportion to area and the LiDAR estimates was r=0.85. At the woodland level, LiDAR estimates were nearly 24% lower than those from the upscaled plot data. This suggests that field-based approaches alone may not be adequate for carbon accounting in heterogeneous forests. Conversely, the LiDAR 20×20 m grid approach has an enhanced capability of monitoring the natural variability of AGCC across the woodland.
© 2004 Elsevier Inc. All rights reserved.

Keywords: Carbon; Forest; LiDAR

1. Introduction

The need to increase the accuracy and the spatial coverage of carbon accounting in forest ecosystems has both political and scientific rationales. Politically, countries ratifying the Kyoto Protocol to the United Nations Framework Convention on Climate Change (UNFCCC) will be required to report annually their direct human induced (DHI) emissions and removals of carbon dioxide (UNFCCC, 1997). The reporting requirements include DHI emissions and removals of carbon dioxide from Land Use, Land Use Change and Forestry activities, which comprise deforestation, afforestation, and reforestation activities (Article 3). In addition to the need to report nationally DHI emissions and removals of carbon dioxide, mechanisms in the Protocol allow countries to implement jointly projects aiming at reducing atmospheric carbon dioxide through Land Use, Land Use Change and Forestry activities (Article 4, Article 12). Estimating DHI carbon dioxide emissions from forestry related activities implies a prior knowledge of the carbon content of the land area, from which net carbon change can be inferred through subsequent

* Corresponding author. Centre for Ecology and Hydrology, Bush Estate, Penicuik, Midlothian, EH26 0QB, UK. Tel.: +44 131 445 4343; fax: +44 131 445 3943.
E-mail addresses: genevieve.patenaude@eci.ox.ac.uk, bu01gp@ceh.ac.uk (G. Patenaude).

0034-4257/$ - see front matter © 2004 Elsevier Inc. All rights reserved.
doi:10.1016/j.rse.2004.07.016

carbon content estimations. However, large uncertainties remain in estimating carbon content both in the above and below ground components of forests due to the spatial coverage of these ecosystems, their heterogeneity and the inherent difficulty to produce field-based inventories at national, continental and global scales. This need to improve carbon content estimates in forest ecosystem is also of scientific interest. Reducing these uncertainties may help in solving the missing terrestrial carbon sink, which is of the order of 1.9 gigaton of Carbon (GtC) annually (Houghton et al., 2001). Several studies suggest that it may be unaccounted for in the temperate and boreal forest regions (Bousquet et al., 2000; Rayner et al., 1999). Thus, accurate, rapid and cost efficient tools are required to improve the estimates of carbon content in temperate and boreal forest ecosystems and to enable countries, or any organisation involved in the nascent carbon-trading scheme to estimate accurately the carbon content of their national or project-related forested lands.

Although field based carbon estimations remain necessary for these purposes, integrating remote sensing into carbon inventory schemes allows recovery of carbon content and spatial interpolation of estimates across landscapes, while reducing the total costs and the need for extensive field-based sampling. Several radar or passive optical remote sensing approaches have already proven adequate for quantifying above ground biomass in relatively homogeneous and young forests (Ahern et al., 1991; Dobson et al., 1995; Franklin et al., 1986; Ranson et al., 1995; Ripple et al., 1991; Fransson & Israelsson, 1999). Unfortunately, these are still inapt for monitoring biomass of mature or heterogeneous forest ecosystems (Holmgren & Thuresson, 1998; Imhoff, 1995). Radar and passive optical remote sensing suffer from a common setback: the signal-to-noise ratio or the sensitivity of these approaches decreases with increasing canopy structural heterogeneity and age. A comparatively recent, active remote sensing technique that operates on a principle called Light Detection And Ranging (LiDAR) has strong potential to monitor forest biomass and volumes across ecosystems and above-ground biomass ranges (Lefsky et al., 1997, Lefsky et al., 1999a, 1999b, Means et al., 1999, 2000; Nilsson, 1996). In addition to being less restricted by weather conditions and sun angle considerations than other optical remote sensing approaches, LiDAR systems provide georeferenced digital elevation at high spatial resolution, with high accuracy and at relatively low costs (for approximate costs, see (www.airbornelasermapping.com). However, in contrast to optical and radar systems, LiDAR devices collect samples along a flight path and as such, are not imaging systems. Interpolation between the sample points is required for thematic mapping. Flood and Gutelius (1997), Wehr and Lohr (1999), and www.airbornelasermapping.com provide good overviews of the conceptual basis and functioning of these systems. Methods for processing the collected data are summarized by Axelsson (1999).

For forestry application, two types of LiDAR systems can be differentiated: discrete-return devices (DRD) and waveform recording devices (WRD). The general specifications of these system types are detailed in Lefsky et al. (2002). Both DRDs and WRDs have been used worldwide for characterising forest structure (Drake et al., 2002, Gaveau & Hill, 2003; Hyyppa et al., 2000, 2001; Lefsky et al., 1999a). These technologies have successfully been used to retrieve tree height (Naesset, 1997a; Magnussen & Boudewyn, 1998; Magnussen et al., 1999), above ground biomass and timber volumes (Naesset, 1997b; Hyyppa et al., 2001) and crown properties (Naesset, 2002, Naesset & Okland, 2002). Lefsky et al. (2002) and Lim et al. (2003) review the potential of LiDAR devices for retrieving forest parameters. Although some studies have investigated their potential for forest carbon accounting (e.g. Drake et al., 2002; Nelson et al., 2003; Omasa et al., 2003), there is still a need to develop methods suitable for temperate and uneven aged, mixed deciduous woodlands. In this paper, we present a method based on DRD LiDAR canopy height measurements for estimating forest above ground carbon content (AGCC) in a semi-natural, deciduous woodland, for which extensive ground based measurements were collected.

2. Data collection

2.1. Study area

Monks Wood National Nature Reserve (NNR) is a 157 ha semi-natural, partly managed, temperate deciduous woodland located at 52°24′ N, 0°14′ E in Cambridgeshire, UK. The dominant tree species are ash *Fraxinus excelsior* L., oak *Quercus robur* L., field maple *Acer campestre* Linn., with some occasional clusters of elm *Ulmus carpinifolia* Gleditsh. and aspen *Populus tremula* Linn. Dominant shrub species include hawthorn *Crataegus monogyna* Jacq., hazel *Corylus avellana* Linn., blackthorn *Prunus spinosa* Linn., dogwood *Cornus sanguinea* Linn., and wild privet *Ligustrum vulgare* Linn. Heavy felling was made in the wood during and after the 1914–1918 war so the majority of overstorey trees are estimated to be aged 70–80 years. The highest part of the reserve rises to about 46 m above sea level with a maximum slope angle of 14.5° (Steele & Welch, 1973).

2.2. Ground based AGCC data (48 plots)

Fieldwork was undertaken in July 2000. Five contrasting stands falling under a specific management class and representative of the woodland were selected (Table 1). These were defined as compartments of trees with relatively homogenous species composition and structure. Each stand was divided into a grid of 10 equal areas (8 in stand 5). One 20×20 m sample plot was located randomly

Table 1
Summary of the stand reference data (modified from Patenaude et al., 2003)

Stand no. [ha]	Woodland area[a]	No. of plots/stand [GPS located][b]	No. of trees per ha (dbh≥7 cm)	Stand basal area (m^2 ha^{-1})	AGCC[c]. (Tonnes ha^{-1})
1 [2.57]	17.07 NI	n=10 [7]	933	31.15	107 (8.2)
2 [3.35]	17.07 NI	n=10 [3]	1113	31.26	92 (6.3)
3 [2.83]	9.00 FG	n=10 [4]	1045	19.75	61 (7.1)
4 [3.69]	57.89 W	n=10 [6]	1008	30.92	85 (7.8)
5 [0.84]	55.76 MC	n=8 [5]	852	70.77	164 (8.8)
Total woodland	156.79 ha	n=48 [25]	Avg. 990	Avg. 36.77	Total: 17.99 ktonnes

[a] Surface area (ha) of Monks Wood, which falls under similar vegetation structure and management class (Steele & Welch, 1973). NI=Non-interference; FG=Fields and glades; W=Woodland; MC=Mixed and coppiced.

[b] Numbers in brackets correspond to the number of plots located using a global positioning system (GPS).

[c] Integrates all woody above-ground and foliage components as well as ground vegetation and litter. Values are means. Standard errors are given in parentheses.

within each of these 10 gridded areas (8 in stand 5). This sampling approach yielded ten 20×20 m sample plots in 4 of the 5 stands, and 8 in stand 5. Only eight sample plots were recorded in stand 5 because of its homogeneity and small size (Patenaude et al., 2003). The plots were selected following the methodology proposed by Hamilton (1975). Not all plots location could be recorded using a hand-held GPS. However, all were located using field-based quantitative description of plot centre locations (distance and orientation from path intersection and/or easily identifiable features).

Monks Wood NNR is a protected reserve so only limited destructive measurements were allowed. The approach summarised here relies primarily on non-destructive forestry mensuration methods and is detailed in Patenaude et al. (2003). For each plot, species and diameter at breast height (DBH) for all woody stems of at least 7 cm DBH were recorded, totalling 2272 trees in 48 plots. Following the approach by Crockford (1987), trees of DBH larger than or equal to 18 cm were defined as overstorey, whereas trees and shrubs between 7 and 18 cm DBH were defined as understorey. A 1×1 m sample of ground vegetation and litter (including trees and shrubs <7 cm DBH) was collected from the centre of each plot. This sample was air-dried and weighed to estimate dry mass (see Patenaude et al., 2003). Belowground vegetation components and soils were not considered here, as these components were not estimated from the LiDAR measurements.

For each overstorey tree per plot, total woody above ground volume was calculated using species-specific regressions developed by Crockford (1987). Species-specific values for wood basic density and carbon content published by the UK Forestry Commission were then used to convert each stemwood volume into carbon content (Hamilton, 1975). Proxy values were used when species-specific values were not available (see Patenaude et al., 2003 for details). Understorey species were dealt with as one unit in each plot and their total dry weights for all shoots per plot were estimated using relationships based on basal area (Crockford, 1987). A conversion figure of 0.49 was then used to convert understorey dry weight to carbon content (Birdsley, 1990; Matthews, 1993). Foliage dry weight was estimated by species for each overstorey tree. For the understorey, foliage dry weight was derived as a percentage of above ground understorey wood dry weight. These foliage conversion factors were derived from a study conducted in an English wood similar to Monks Wood NNR in terms of species composition and environment (Satchell, 1971). The carbon content for the foliage, ground vegetation and litter was then assumed to be 45% of dry weight, a figure commonly used for foliage, herbs and litterfall (Ajtay et al., 1979; Vogt, 1991). Table 1 summarises the field data collection and the resulting AGCC estimates per stand. For further information on the ground based AGCC estimation in Monks Wood, see Patenaude et al. (2003).

2.3. LiDAR ground elevation (1-m grid) and canopy elevation (1-m grid)

On the 10th of June 2000, a DRD, small footprint Airborne Laser Terrain Mapper (Optech ALTM 1210) was flown over the Monks Wood NNR, in a north–south direction. The ALTM emits laser pulses at wavelength 1047 nm (see unit Table 3) (near infrared); part of the electromagnetic spectrum at which vegetation is highly reflective. The precision of the instrument was approximately 0.60 m in the x and y position and 0.15 in z (Gaveau & Hill, 2003, www.optech.on.ca). Table 2 summarises the specifications of the ALTM flight and data collection. The scanning orientation, perpendicular to the flight direction, generated a saw-toothed sampling pattern. This, together with overlapping and combined flight paths produced an irregular distribution of laser footprints (Table 2). For each point sample, only the first and last significant returns were considered, corresponding to the first and last part of the recorded signal.

Elevation attributes of the first and the last significant returns were treated as separate data sets. Interpolation of elevation attributes from the point-clouds of the first and last-returns to two spatially continuous surfaces was achieved in two stages. Firstly, a Triangulated Irregular

Table 2
Summary of the LiDAR and flight data

System	Wavelength	Significant returns recorded	Footprint diameter at nadir	One ground canopy hit per:			Scan angle
				Min[a]	Max[b]	Mean[c]	
Optech ALTM 1210	1047 ηm	First and last	0.25 m	2.80 m^2	6.50 m^2	4.83 m^2	±10°

[a] In areas scanned with overlapping flightlines.
[b] In areas sampled in one flightline.
[c] Mean across the woodland.

Network (TIN) based on a Delaunay triangulation was applied to each dataset. Secondly a rectangular grid of pixels was extracted from each TIN using a linear interpolation method at a constant sampling interval of 1 m to generate the surfaces. This created a 1×1 m spatial resolution raster for each surface. The surface layer created from the first return was assumed to approximate canopy surface elevations. The layer generated from the last return was assumed to be from ground surfaces or surfaces located beneath or within the canopy. From these, a Digital Canopy Height Model (DCHM) and a Digital Terrain Model (DTM) were generated as described below. A clear distinction between elevations and heights is made here. Whereas elevations are given in meters above sea level (ASL), height is the vertical distance between two points (e.g. ground and tree canopies).

To generate the DTM from the last return surface layer, differentiating between returns from the ground and surfaces located from within the canopy was crucial. Several methods have been proposed (e.g. Kilian et al., 1996, Ruppert et al., 2000). Here, an adaptive morphological filter was applied to identify local minima, varying the filter size according to canopy structural heterogeneity. Enlarging the filter size where fewer canopy gaps were present increased the probability of locating local minima. Where the canopy was more open, smaller filter sizes were selected (Hill et al., 2003). A thin plate spline interpolation process was then applied to render a terrain surface from extrapolating between the extracted local minima (Hill et al., 2003). This method of interpolation fits a smooth (continuous and differentiable) minimum curvature surface passing through all input point data. To generate the Digital Canopy Height Model, the DTM (corrected for bias, Section 3.1) was subtracted on a per pixel basis from the canopy elevation layer created from the first return.

2.4. Theodolite ground elevation (244 points) and canopy elevation (82 points)

Reference elevation data were recorded in June 2000 using a Pentax R-125N electronic total station (laser theodolite) which has a ranging distance, D (meters), of accuracy $0.005+0.003D$. For each observation, the x, y and z position was calculated in relation to a permanent Ordnance Survey (OS) benchmark located at the Centre for Ecology and Hydrology (CEH) Monks Wood research station. The elevation values (z) were calculated in meters ASL, in relation to the OS 1936 Datum for Great Britain.

A total of 326 reference point measurements were collected, comprising 244 terrain elevation samples, recorded under the canopy and along exposed paths (rides), and 82 shrub and tree canopy elevation measurements. These three datasets (terrain, shrubs, trees) were collected in different locations due to the logistics of data collection. For the terrain and shrubs, the total station was operated from the ground. The network of rides enabled access to the wood with the total station and a series of radial points to be recorded. Among the terrain elevation samples, 140 were taken under the canopy while 104 were alongside rides, locating the prism on a pole of known height. For shrub canopy elevation, the prism was attached to an 8-m extendible pole. A total of 43 shrub canopy elevation samples were taken, 34 of which were along a 275-m transect. For the tree canopy elevation, the total station was located at the top of a 15-m tower situated at the research centre of CEH Monks Wood. An 18-m truck-mounted platform was used to provide access to upper canopies and to locate the prism. A total of 25 of the 39 tree canopy elevation samples were located along a 275-m transect that was easily accessible with the apparatus. All samples of tree and shrub canopies were collected at the edge of the wood. For all canopy samples, the reflecting prism was located at random on crown upper surfaces not necessarily representing crown apexes, thus measuring canopy elevation rather than tree elevation in a similar way to the LiDAR method. Further information on the acquisition of the reference data sets are detailed in Gaveau and Hill (2003).

2.5. Drymass density (49 trees)

An assessment of dry mass density in Monks Wood was made from coring samples of dominant tree species. The sampled trees were selected so that their DBH was roughly that of 25±10 cm. Assuming unmanaged conditions and low productivity, this is the typical DBH for these trees species when aged between 70 and 80 years (the average tree age in Monks Wood) (Edwards & Christie, 1981). A total of 49 trees were cored, from which tree rings were counted to estimate age. Dry mass density from these tree cores was estimated for all overstory tree species (Table 3). The species averages with standard errors were used to

Table 3
Summary of 48 plots for calibration of the carbon model

Tree species	Ash	Maple	Oak	Others	Total[a]
Tree count in all plots	838	239	138	1057	2272
[Relative frequency, all trees considered][b]	[36.9%]	[10.5%]	[6.1%]	[46.5%]	[100.0%]
Relative frequency, dominant species only[b]	69%	20%	11%	–	–
All tree species basal area (m^2 ha^{-1})	21.9	5.8	13.8	21.7	63.2
[Relative frequency, all trees considered][b]	[34.7%]	[9.2%]	[21.8%]	[34.3%]	[100.0%]
Relative frequency, dominant species only[b]	52.9%	13.9%[c]	33.3%	–	–
Tree density (g cm^{-3})[d]	0.70	0.61	0.68	–	0.68[e]
[Relative standard error]	[0.97%, n=27]	[1.61%, n=10]	[1.70%, n=12]		[5.8% n=6][c]

[a] Includes all trees and shrubs≥7 cm DBH.
[b] n=48 plots.
[c] Value in bracket is the weighted standard deviation of species averages.
[d] Trees of DBH=25 cm±10 cm were sampled, corresponding roughly to trees between 70 and 80 years of age (Edwards & Christie, 1981, refer to text).
[e] Weighted average from birch, elm, aspen, oak, ash and maple (weight: basal area).

construct a weighted mean and weighted standard deviation of means for the whole wood. The basal area of each species was used as weight (Table 3).

3. Modelling

3.1. Ground elevation (244 points)

Table 4, Fig. 1 and Fig. 2 present the summary statistics resulting from the comparison between the reference and the LiDAR elevation and height datasets (DTM and DCHM).

Although Fig. 1a shows a close agreement between the DTM and the reference elevation data, the DTM overestimates reference by an average of 0.23 m (significantly different from 0, $p \ll 0.001$, two-tailed t-test) (Table 4 column a, Fig. 1b). The difficulty of generating DTMs under dense canopy covers using LiDAR data has been widely recognized (Blair et al., 1999). Accurate DTM generation will be a function of sampling density, scanning angle, canopy density and canopy closure, and processing methods (Gaveau & Hill, 2003). Here, even if an adaptive morphological filter was applied to locate the local minima (from which the DTM was generated), the majority of last returns may have been reflected from surfaces above the ground, generating this overall overestimation of the reference elevation data. The DTM was thus calibrated by subtracting the systematic offset from pixel elevation values of the DTM.

Table 4
Summary statistics of residuals in the DTM and the DCHM (Modified from Gaveau & Hill, 2003)

	a. DTM	b. DCHM	
		Shrubs	Trees
Range	−1.78 to +1.65	−2.50 to −0.05	−5.23 to +0.11
Mean	+0.23	−1.02	−2.12
SE	2.9%	19.8%	7.1%
n=	244	43	39

Minus and positive signs equate to an underestimation and overestimation of the reference data elevation, respectively.

3.2. Canopy height (82 points)

Table 4 (column b) presents statistics for the height residuals from the LiDAR DCHM. Canopy heights for the reference and the LiDAR canopy elevation were obtained by subtracting the calibrated DTM from both datasets (the latter yielding the DCHM). As shown in Fig. 2, the DCHM consistently underestimates reference heights. Tree height underestimation using small footprint DRD LiDAR is not uncommon and is a function of several factors internal and external to the study site (Gaveau & Hill, 2003; Hyyppa et al., 2000; Lefsky et al., 2002). Internal factors include the canopy structure (conical or spherical shapes) and the canopy density (plant surface area, perpendicular to illumination angle, per surface area). External factors include the configuration of the LiDAR system used as well as the sampling design. For example, high sampling density or large footprint sizes will increase the probability of sampling tree apexes. Other external factors include the strength and wavelength of the output signal, which will influence the strength of the returned signal; the threshold detection selected which defines how strong the return signal must be to trigger a recording; and the signal-to-noise ratio sensitivity (Gaveau & Hill, 2003; Hyyppa et al., 2000; Lefsky et al., 2002). Here, internal factors are an important source of canopy height underestimation. As shown in Fig. 2 and Table 4b, height underestimation increases as a function of canopy height. As Gaveau and Hill (2003) suggested, canopy density and structure variations across species, rather than height, is the main factor for height underestimation in Monks Wood. They noted that shrub species had a higher canopy density than trees. As such, the signal was less likely to penetrate deep into the shrub canopy before encountering sufficient matter to return a first significant signal (thus reducing height underestimation). Here, as no information on species is available per pixel in the DCHM, height is taken as a surrogate to differentiate trees and shrubs.

To calibrate the DCHM, alternatives to the use of standard linear regressions must be sought because both

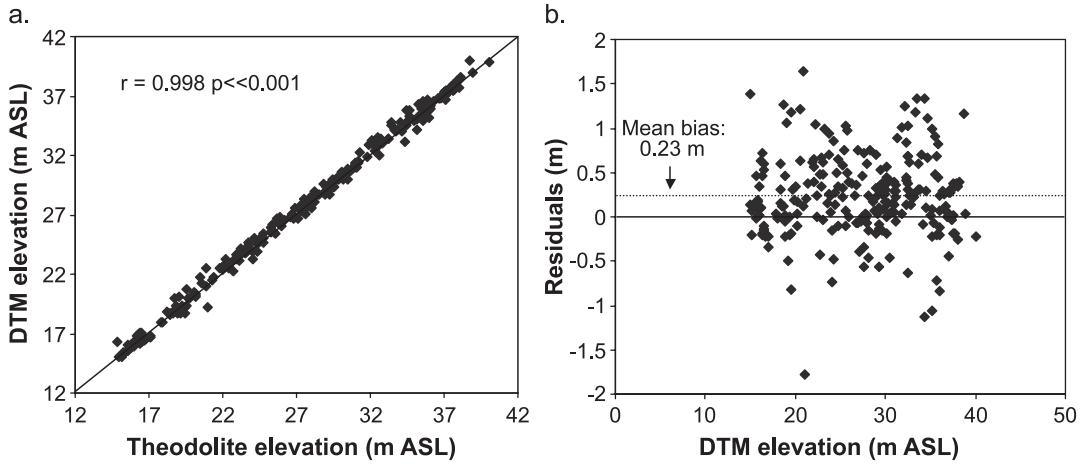

Fig. 1. (a) Digital terrain model (DTM) against reference elevation data (m above sea level, ASL). (b) Digital terrain model (DTM) residuals (m).

the reference and LiDAR datasets are measured with errors (Snedecor & Cochran, 1980). Additionally, the variances of tree and shrub height residuals are heteroscedastic (statistical distributions with different variances, Fig. 2). Both systematic and random errors appear to be a function of height and canopy density (the larger the trees, the larger the mean and variance of residuals). Statistical analyses supported these observations as significant differences were found to exist between averages of tree and shrub canopy height residuals (t-test, $p \leq 0.001$) and between variances of tree and shrub height residuals (F-test, $p \ll 0.001$).

Assuming that the variance of residuals is proportional to the theodolite canopy height (H_R) and that height is an acceptable surrogate for differentiating between the canopy densities of trees and shrubs, it is reasonable to use the ratios of means as the slope to the equation for calibrating the DCHM (Snedecor & Cochran, 1980). The model below was used to calibrate all pixels in the DCHM (Eq. (1), Fig. 2).

$$H'_{\mathrm{DCHM}} = bH_{\mathrm{DCHM}} \quad (1)$$

where: b=1.19= $\Sigma H_R/\Sigma H_{\mathrm{DCHM}}$; H'_{DCHM}= Calibrated pixel height; H_{DCHM}= Pixel height; H_R= Theodolite canopy height.

After calibration, all 48 ground plots were located on the calibrated DCHM using the GPS coordinates available combined with the quantitative description of the location of the centre of each plot. From each centre coordinate, a circular plot of 20 meters diameter was overlaid on the DCHM.

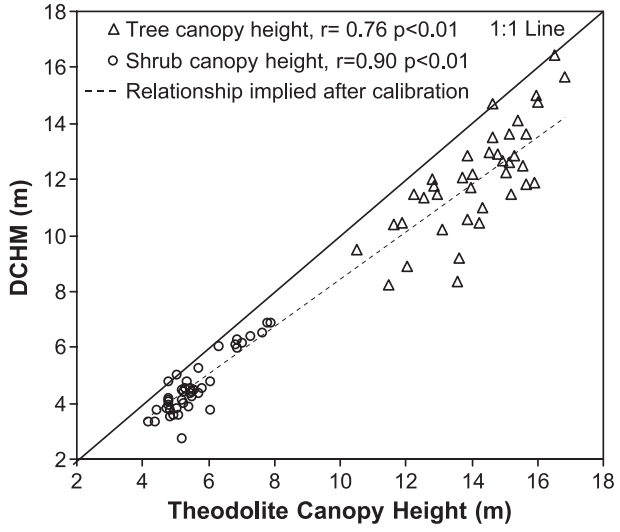

Fig. 2. LiDAR against reference canopy height estimates (m).

3.3. Basis for a carbon model

Although canopy height variables are available from LIDAR, these are not the most commonly used predictors of above ground biomass, volume or AGCC. Rather, tree diameter or stand basal area is most frequently utilised. However, height metrics have been used successfully as a surrogate for these variables when basal area or DBH were not available (Nelson et al., 1988; Naesset, 1997b, 2002). A form for the AGCC model using height metrics as a predictor was therefore developed from forestry yield tables. The starting point was a model predicting stemwood volumes from height derived from Sycamore-Ash-Birch Yield (SAB) production tables (Edwards & Christie, 1981). These tables provide empirical growth data and models for plantation stands, relating stand variables such as dominant height (the average height of the 100 trees with largest DBH per hectare) to merchantable stemwood volume on a per hectare basis. Although yield tables were designed for plantations, they were selected here due to their wide availability and adaptability given UK environmental conditions and forest types.

For deciduous species, a limited number of yield tables were available: Oak; Sycamore-Ash-Birch (SAB); Beech;

Hybrid poplars; and Southern Beech (Edwards & Christie, 1981). The SAB tables were selected because ash is by far the most dominant species in Monks Wood. As shown in Table 3, ash contributes to more than 34% of the total basal area in the 48 plots and to nearly 37% of the population of all trees ≥7 cm DBH. Maple is also a common species at Monks Wood; nearly half of the total tree population in the 48 plots is composed of ash and maple. Since sycamore is an acceptable proxy for maple (Edwards & Christie, 1981), the selection of the SAB yield tables appears appropriate. The equation (model) relating stemwood volume to a height variable was then modified by incorporating a conversion factor (Total tree carbon per stem volume) to estimate AGCC.

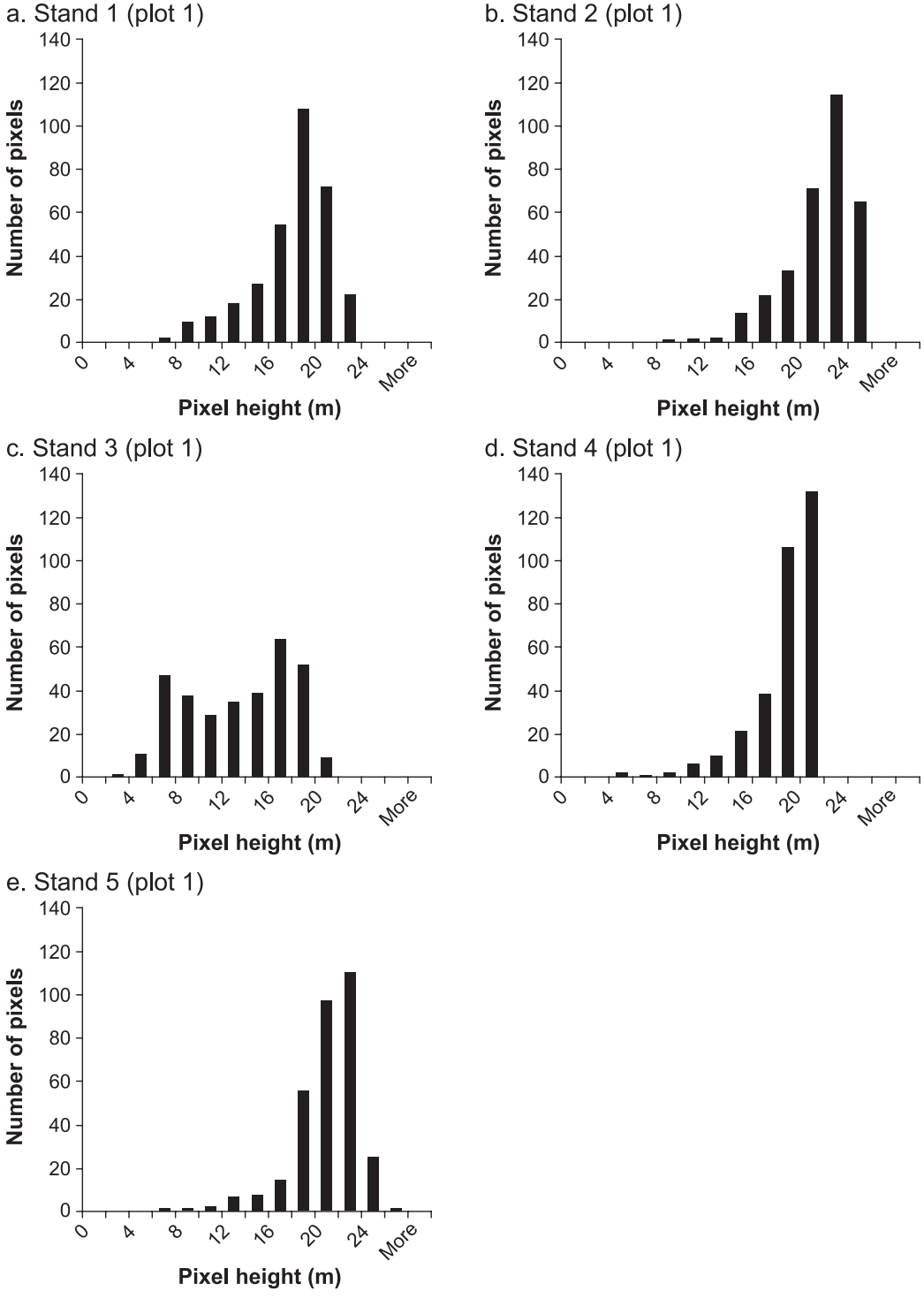

Fig. 3. Height distribution of plots from the five stands.

The form of the equation selected thus uses a LiDAR height metric ($H_{\%}$) as predicting variable and is as follows:

$$\mathrm{AGCC} = kae^{bH_{\%}} \quad (2)$$

where the parameter k converts stemwood volumes to total AGCC (Table 5) and is derived from empirical conversion factors available in the literature (Dewar & Cannell, 1992; Milne et al., 1998; Salway et al., 2001). Parameters a and b are site-specific and optimised against ground data (detailed below). Specifically, a represents the initial volume (m^3 ha^{-1}) found when $H_{\%}$ equals 0. This parameter enables to take into consideration the AGCC present in the ground vegetation and litter compartment when no height is "recorded" by the LiDAR; in Monks Wood, between 2.3 and 4.6 tonnes ha^{-1} is found in ground vegetation and litter only (Patenaude et al., 2003). The b parameter can be considered as an indicator of the productivity of the site. Finally, $H_{\%}$ is derived from the LiDAR DCHM and is a variable surrogate to dominant height. Relying on a variable characteristic of a stand possesses the advantage of removing the need to identify individual trees from the LiDAR dataset. Estimates of total stemwood volumes and AGCC on a per hectare, rather than on a per tree basis are provided, given that an appropriate height metric characteristic of the stand is provided. Although dominant height is a suitable variable for characterising the height distribution of plantation stands, this variable would be inappropriate for a mixed deciduous woodlands such as Monks Wood as it may not reflect height distributions where trees are of mixed species and ages as it does for plantations. To select an appropriate height statistic ($H_{\%}$) representative of Monks Wood, height distributions for the 48 measured plots were plotted. A sub sample is presented in Fig. 3.

Of the 48 height distributions, most were skewed to the left and a few were bimodal. Thus, as the model presented in Eq. (2) is exponential, the average height per plot would underestimate the weight of larger trees and shrubs on the AGCC of most plots. Likewise, the maximum height would disregard smaller trees; the AGCC in a plot with a majority of shrubs and one large tree would be significantly overestimated. Bimodal distributions render the mode an inappropriate statistic. Various percentiles of heights, selected to be above the median to seize the bulk of the distributions, were therefore chosen and tested as a best statistic descriptive of height distributions. This approach is not dissimilar to that proposed by Naesset (1997a) and Magnussen and Boudewyn (1998) which used percentiles of LiDAR height estimates in coniferous plantations as estimators of average stand height.

The selection of the parameters a and b together with an appropriate height statistic ($H_{\%}$), was carried out by means of optimisation against ground data. The field-based estimates of AGCC were plotted against spatially corresponding

Table 5
Optimised model parameters for Monks Wood

Parameters to optimised model			Notes
	a	19.186	At height 0, an initial volume of 19.186 m^3 ha^{-1} (equivalent to approximately 4 tonnes ha^{-1} of carbon) is assumed. This is not unreasonable, as carbon content in ground vegetation and litter range between 2.3 and 4.6 tonnes ha^{-1} in Monks wood (Patenaude et al., 2003).
	b	0.1256	
$k=dgh$	d	1.36	Biomass expansion factor for UK deciduous forests. Converts stemwood volume to total above ground volume.[a]
	g	0.68	Dry mass conversion factor. Converts volume to dry mass (Table 3).
	h	0.49	Carbon content conversion factor. Converts dry mass to carbon content for UK deciduous forests.[a]

[a] Conversion and biomass expansion factors in Dewar and Cannell (1992), Milne et al. (1998) and Salway et al. (2001).

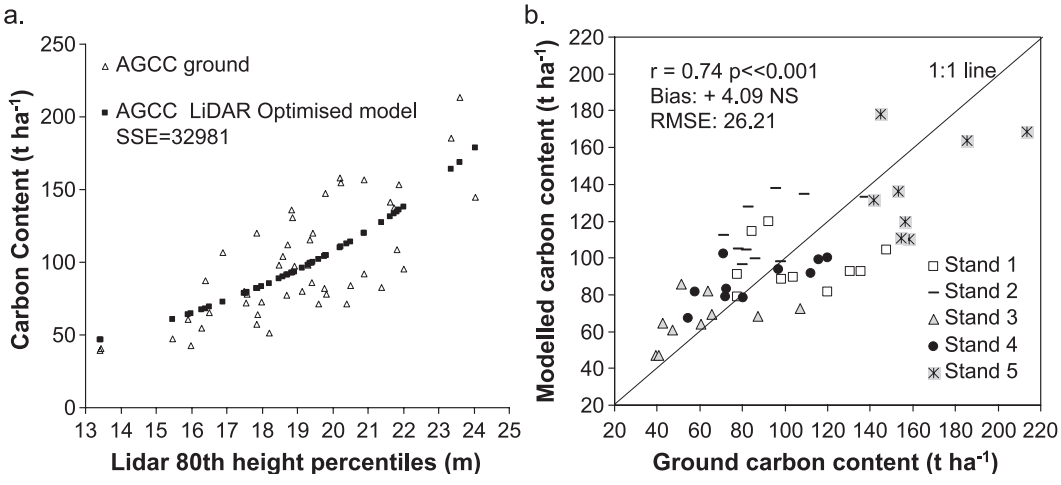

Fig. 4. (a) Field-based AGCC and AGCC from optimised model against the LiDAR 80th height percentiles (at the plot level). (b) AGCC from optimised model against field-based estimates (at the plot level). AGCC=Above-Ground Carbon Content; SSE=Sum of Square Errors.

Table 6
Sum of square errors (SSE) between modelled and field-based AGCC

Parameters and SSE	Height statistics			
	Average	60th percentile	80th percentile	Max
a	38.308	24.620	19.186	15.349
b	0.1182	0.1231	0.1256	0.1322
SSE	35,798	33,765	32,981	34,757

Various statistics for fine-tuning the carbon model have been tested. The 80th percentile, which generated the lowest SSE, was selected.

height statistics from the DCHM (e.g. average height, 60th percentile, 80th percentile, maximum height) (Fig. 4a). For each statistic, a and b were varied to provide the best fit and lowest Sum of Square Error (SSE) between the modelled AGCC and the field-based estimates of AGCC. The best results were obtained with the 80th percentile and the parameters values presented in Table 6. SSEs are also shown. This statistic, conversely to the average or the maximum height, confers a larger weight to taller trees (which account for a larger portion of the AGCC) without disregarding the contribution of smaller trees. Coincidentally, the 80th percentile was also nearest to the mode for the majority of height distributions. In Fig. 4a, two datasets are plotted against the 80th percentile: firstly, the ground-based estimates of AGCC; secondly, the optimised AGCC obtained from the fine-tuned model (Tables 5 and 7). Fig. 4b shows the correspondence between the field-based AGCC and the modelled AGCC for all plots (Table 6).

3.4. Stand and woodland AGCC

Each of the five stands in the DCHM was divided into a grid of 20×20 m cells ($n \geqslant 10$ per stand), the cell size corresponding to the dimensions of the plots used in ground-based sampling. For each grid cell, the 80th height percentile was extracted. This approach aims at capturing a maximum of variability within stands and within the whole woodland. The AGCC in tonnes per hectare for all grid cells was then averaged per stand. The same procedure was applied across the woodland to provide AG carbon density and total carbon content.

4. Results and discussion

Fig. 4b shows the AGCC modelled from 80th percentiles plotted against field-based estimates of AGCC for all coincident plots. Overall, the agreement between the two approaches is good (r=0.74, $p \ll 0.001$). Although the modelled AGCC overestimated ground estimates by 4.09 tonnes ha^{-1} on average, this bias is not significantly different from zero (t-test, $0.01 \geq p > 0.001$, n=48). The RMSE is small (26 tonnes ha^{-1}) considering that these approaches are compared at the plot level, where the inter-plot variability is high.

The results at the stand and woodland level are presented in Fig. 5, Fig. 6 and in Table 7. At the stand level, the correspondence between the field-based estimates of AGCC scaled up in proportion to area and those derived using the 20×20 m grid approach is good. The correlation is high (r=0.85) although significant only at $0.1 \geq p > 0.05$ possibly due to the small number of stands considered (n=5). LiDAR stand estimates are within 14% of the ground-recorded stand estimates, except for Stand 2, where LiDAR estimates are 33% larger than that from the ground. On average, the estimates from the grid approach are 3.54 tonnes ha^{-1} lower than the ground estimates but this bias is not significantly different from zero (t-test, $0.05 \geq p > 0.01$, n=5). This suggests that both methods are equally able to capture the AGCC and its spatial variation within each stand.

At the woodland level however, the AGCC estimates from the ground (n=48) and the grid approach (n=3638) contrast considerably (Table 7, columns a and b). The LiDAR grid estimate is lower than the ground-based estimates of total woodland AGCC by 23% (nearly 4000 tonnes). The differences between the two approaches at the plot and at the stand level are insignificant but are considerable at the woodland level. This implies that differences in estimates for the entire woodland do not arise from the accounting methods but rather, from the scaling approach used and the poor representation by the selected stands of the rest of woodland. To assess this, only the AGCC estimates from the 48 plots on the DCHM were considered to estimate the total woodland AGCC by using the same upscaling method as the ground based approach i.e. for both approaches, n=5 stands of 8–10 plots each. As shown in column a and c of Table 7, the resulting LiDAR estimate is of comparable magnitude to the field-based estimate (4.4% below the field-based value). Thus including all pixels grouped under 20×20 m grids increases the accounting of the natural variability of AGCC within the

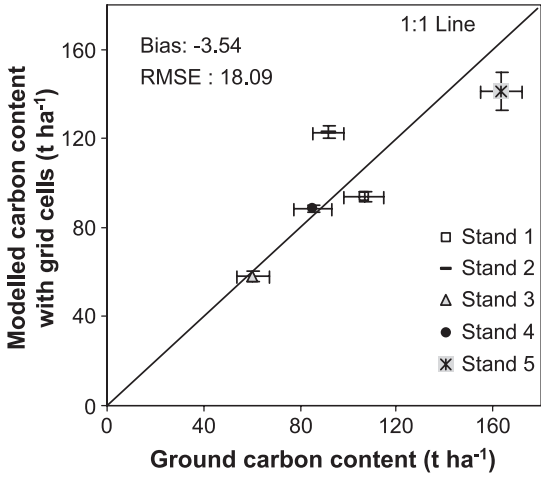

Fig. 5. AGCC per stand using all grid cells ($n \geqslant 10$ per stand) against AGCC from upscaled ground-based plot data ($8 \leq n \leq 10$). Error bars are standard errors.

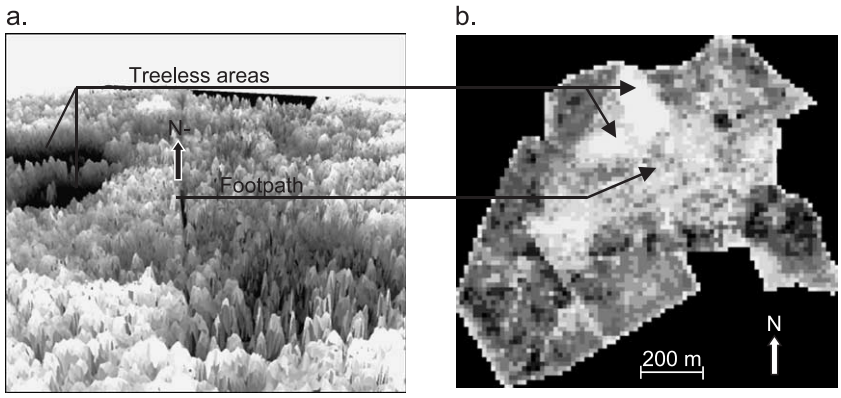

Fig. 6. (a) 3D view within the resulting DCHM. Gradients from black to white correspond to heights between 0 and 26 m, respectively. (b) Final AGCC map of Monks Wood (tonnes ha^{-1} per 20×20 m cells). Dark areas indicate high AGCC (max: 215 tonnes ha^{-1}) and pale, low AGCC (min: 8 tonnes ha^{-1}).

woodland. Whereas variations within the stands are captured similarly by both approaches (as shown in Fig. 5), the within-woodland heterogeneity appears to be better captured by the LiDAR approach (Table 7). Treeless areas as well as path networks within the woodland are not accounted for in the ground sampling because these do not feature in the literature on the management of the woodland (path surface areas are merged to other management classes). The ground sampling approach relies on the assumption that the plots are representative of the stands, and the stands, of all woodland areas falling under the same management class. The high cost of fieldwork is usually prohibitive in producing detailed assessments of AGCC in structurally heterogeneous forests. Clearly, these treeless areas could be easily removed if their location were known using a GIS database. However, these are not always available and areas identified in a GIS database as forests may not appear as such in reality. LiDAR methods sample across the woodland rapidly and at high sampling density, thus acquiring data on variability.

The approach used is sensitive to the spatial scale of this analysis. Selecting the 80th percentile per 20×20 m grid cell and calculating the AGCC for each grid cell from this percentile will not yield the same result as selecting the 80th percentile of the woodland and calculating the AGCC of the woodland based on a single height estimate. If the carbon model were linear, the model would be independent of the selected scale because the contribution of heights is distributed proportionally. The exponential nature of the carbon model confers larger weights to larger 80th percentile height values. An alternative approach to the use of percentiles would be to model height distributions across the stands, the woodland, or any area of interest. Weights for the AGCC estimates per height class would be provided according to the modelled height distribution. Such an approach would increase the accuracy of predictions in areas exhibiting non-Gaussian or bimodal height distributions. Additionally to the sensitivity of the approach, care should be taken in the use of exponential models. Although the model described here has an appropriate shape, it should only be applied to the range where it was fitted.

Table 7
Total above ground carbon content estimate of Monks Wood from different approaches (see text)

	a. Field-based AGCC (Plot data only)	b. LiDAR estimated AGCC (All grid cells)	c. LiDAR estimated AGCC (Plot data only)
Total woodland carbon content (ktonnes)	17.99	13.88	17.21

The results obtained here are comparable to those from similar studies making use of LiDAR to characterise above-ground biomass or volume in coniferous forest ecosystems. Unfortunately, very few studies have focussed on quantifying theses variables in temperate deciduous woodlands. Successful LiDAR estimates of forest variables have been achieved using WRD. The coefficient of determination between LiDAR derived variables and forest biomass or volume range between 0.78 and 0.96, in the studies by Nilsson (1996), Lefsky et al. (1997), Lefsky et al. (1999a,b) and Means et al. (1999). Estimates using small footprint LiDAR have also yielded good results. Whereas only 0.53 of the ground biomass variance could be explained by metrics derived from LiDAR height measurements in mixed hardwood forests (Nelson et al., 1988), the approach used by (Naesset, 2002) explained more than 80% of the ground variations in volume for coniferous forests in Norway, and reached r^2=0.91 when the models were used for prediction purposes.

The literature on carbon accounting using LiDAR approaches is however limited. Using a helicopter mounted WRD, Drake et al., 2002 estimated the carbon content of various land covers in the Costa Rican landscape. At the plot level (0.05–0.25 ha), metrics derived from the LiDAR dataset explained between 89% and 93% of the variation in ground biomass estimates. These results have also

demonstrated the non-saturating capabilities of WRD for carbon assessment across a variety of landscapes. Omasa et al. (2003) proposed a carbon accounting approach for all trees in Japanese coniferous forests, using a small footprint DRD. Carbon was estimated on a per tree basis. The approach yielded excellent results (r^2=0.93) but is inapt for large scale monitoring due to the intensive data requirement. It is clear that LiDARs have improved capabilities for monitoring 3-dimensional forests structure, biomass and carbon content. As long as there is no LiDAR on a satellite platform, it will be problematic to use LiDAR techniques for national scale carbon inventory and for improving our knowledge of the carbon cycle at broad scales. Until then, because WRD remain at a research stage and are still unavailable for commercial and operational use, most local to regional scale carbon accounting from LiDAR technology will need to use the easily accessible and low costs DRD.

Although this method provides a basis that may apply to similar forests elsewhere, further work is required on how implementation of the model may vary for different woodlands. Furthermore, for improving accuracy in above ground carbon accounting from this approach, two difficulties remain to be tackled. Firstly, under dense canopies, the DTMs generated from LiDAR measurements tend to overestimate the actual ground elevation. If no ancillary data are available from which DTMs can be derived or adjusted, this overestimation can be minimised by dual flight campaign strategies. In temperate deciduous ecosystems, the DTM data collection could be planned during winter seasons after leaf fall, whilst DCHM data collection could be projected for summer periods, when the canopy density is at its highest. The second difficulty lies in the consistent underestimation of canopy heights as discussed in Section 3.2. The selection of an appropriate canopy height metric, accounting for some of the underestimation may help in alleviating this underestimation. However, because low canopy density is potentially the main factor for canopy height underestimation in temperate broadleaf woodland (Gaveau & Hill, 2003), further investigation is required to develop systematic monitoring of canopy density to relate this variable to LiDAR height underestimations.

Ultimately, as with all other remote sensing approaches, LiDAR is restricted to above-ground estimations of carbon content in forests. The soil carbon pool combined with the underground vegetation components, such as fine and coarse root systems, represent the largest carbon store in forest ecosystems. For these stores, ancillary data, field-based estimation and modelling techniques will still be necessary for comprehensive carbon accounting. Clearly, these need to be used synergistically for complete accounting, as neither remote sensing, nor ground-based approaches alone can fulfil either the national scale reporting requirements of the Kyoto protocol or the scientific need to account for the missing carbon sink.

5. Conclusions

We have proposed a method for estimating AGCC in a temperate forest in the UK. Further work is nevertheless required to investigate the implementation of the model in different woodlands. Using this approach, no distinction between individual trees is required. Additionally, tree height is not a key variable here. Rather, the approach relies on the extraction of a canopy height statistic, such as percentiles, that is characteristic of the height distributions at the scale of the analysis. Furthermore, the approach makes use of widely available forestry yield table databases.

The results shown illustrate once more the need for combining remote sensing to ground surveying methods for carbon accounting. Whereas ground approaches allow for detailed but spatially limited AGCC quantification, remote sensing permits the scaling of these estimates to larger areas and the monitoring of areas not accounted for using ground based approaches exclusively. Moreover, because the sensitivity of radar and passive optical approaches to biomass or AGCC decreases with increasing canopy structural heterogeneity and age, the potential of LiDAR techniques in such context should be stressed. Both politically and scientifically, there are unambiguous incentives for supporting research and development into DRD or WRD LiDAR missions for carbon accounting purposes.

Acknowledgements

We are grateful to Thomas Brown for his invaluable help in processing the LiDAR data. This project is funded by the British National Space Centre-Link Carbon Offset Verification project, the Biffaward initiative and the Fonds Québécois de la Recherche sur la Nature et les Technologies.

References

Ahern, F. J., Erdle, T., Maclean, D. A., & Kneppeck, I. D. (1991). A quantitative relationship between forest growth-rates and thematic mapper reflectance measurements. *International Journal of Remote Sensing*, *12*, 387–400.

Ajtay, G. L., Ketner, P., & Duvigneaud, P. (1979). Terrestrial primary production and phytomass. In B. Bolin, E. T. Degens, S. Kempe, & P. Ketner (Eds.), *The global carbon cycle* (pp. 129–181). Chichester, UK: Wiley.

Axelsson, P. E. (1999). Processing of laser scanner data-algorithms and applications. *ISPRS Journal of Photogrammetry and Remote Sensing*, *54*, 138–147.

Birdsley, R. A. (1990). Potential changes in carbon storage through conversion of lands to plantation forests. *North American Conference on Forestry Response to Climate Change*, Washington, D.C., 446 p.

Blair, J. B., Rabine, D. L., & Hofton, M. A. (1999). The Laser Vegetation Imaging Sensor: A medium-altitude, digitisation-only, airborne laser altimeter for mapping vegetation and topography. *ISPRS Journal of Photogrammetry and Remote Sensing*, *54*, 115–122.

Bousquet, P., Peylin, P., Ciais, P., Le Quere, C., Friedlingstein, P., & Tans, P. P. (2000). Regional changes in carbon dioxide fluxes of land and oceans since 1980. *Science*, *290*, 1342–1346.

Crockford, K. J. (1987). *An evaluation of British woodlands for fuelwood and timber production*. Ph. D. Thesis, Department of Plant Sciences, University of Oxford. 219 p.

Dewar, R. C., & Cannell, M. G. R. (1992). Carbon sequestration in the trees, products and soils of forest plantations: An analysis using UK examples. *Tree Physiology*, *11*, 49–71.

Dobson, M. C., Ulaby, F. T., Pierce, L. E., Sharik, T. L., Bergen, K. M., Kellndorfer, J., et al. (1995). Estimation of forest biophysical characteristics in Northern Michigan with Sir-C/X-Sar. *IEEE Transactions on Geoscience and Remote Sensing*, *33*, 877–895.

Drake, J. B., Dubayah, R. O., Clark, D. B., Knox, R. G., Blair, J. B., Hofton, M. A., et al. (2002). Estimation of tropical forest structural characteristics using large-footprint LiDAR. *Remote Sensing of Environment*, *79*, 305–319.

Edwards, P. N., & Christie, J. M. (1981). Yield models for forest management. *Forestry Commission*, *vol. 48*. London: HMSO.

Flood M., Gutelius B. (1997). Commercial implications of topographic terrain mapping using scanning airborne laser radar. *Photogrammetric Engineering and Remote Sensing*. 63:327-29,363-66.

Franklin, J., Logan, T. L., Woodcock, C. E., & Strahler, A. H. (1986). Coniferous forest classification and inventory using landsat and digital terrain data. *IEEE Transactions on Geoscience and Remote Sensing*, *24*, 139–149.

Fransson, J. E. S., & Israelsson, H. (1999). Estimation of stem volume in boreal forests using ERS-1 C- and JERS-1 L-band SAR data. *International Journal of Remote Sensing*, *20*, 123–137.

Gaveau, D. L. A., & Hill, R. A. (2003). Quantifying canopy height underestimation by laser pulse penetration in small-footprint airborne laser scanning data. *Canadian Journal of Remote Sensing*, *29*, 650–657.

Hamilton, G. J. (1975). Forest mensuration handbook. *Forestry Commission Booklet*, *vol. 39*. London: HMSO.

Hill, R. A., Hinsley, S. A., Bellamy, P. E., & Baltzer, H. (2003). Ecological applications of airborne laser scanner data: Woodland bird habitat modelling. *Scandlaser conference proceedings, Umeå, Sweden* (pp. 78–87).

Holmgren, P., & Thuresson, T. (1998). Satellite remote sensing for forestry planning—a review. *Scandinavian Journal of Forest Research*, *13*, 90–110.

Houghton, J. T., Ding, Y., Griggs, D. J., Noguer, M., van der Linden, P. J., Xiaosu, D., Maskell, K., & Johnson, C. A. (Eds.). (2001). *Climate change 2001: The Scientific Basis. Contribution of working group I to the third assessment report of the intergovernmental panel on climate change*. Cambridge, UK: Cambridge University Press, 944 p.

Hyyppa, J., Hyyppa, H., Inkinen, M., Schardt, M., & Ziegler, M. (2000). Forest inventory based on laser scanning and aerial photography. *Laser Radar Technology and Applications V.* (pp. 106–118).

Hyyppa, J., Kelle, O., Lehikoinen, M., & Inkinen, M. (2001). A segmentation-based method to retrieve stem volume estimates from 3-D tree height models produced by laser scanners. *IEEE Transactions on Geoscience and Remote Sensing*, *39*, 969–975.

Imhoff, M. L. (1995). Radar backscatter and biomass saturation-ramifications for global biomass inventory. *IEEE Transactions on Geoscience and Remote Sensing*, *33*, 511–518.

Kilian, J., Haala, N., & Englich, M. (1996). Capture and evaluation of airborne laser scanner data. *International Archives of Photogrammetry and Remote Sensing*, *53*, 193–203.

Lefsky, M. A., Cohen, W. B., Acker, S. A., Parker, G. G., Spies, T. A., & Harding, D. (1999a). LiDAR remote sensing of the canopy structure and biophysical properties of Douglas-fir western hemlock forests. *Remote Sensing of Environment*, *70*, 339–361.

Lefsky, M. A., Cohen, W. B., Acker, S. A., Spies, T. A., Parker, G. G., & Harding, D. (1997). LiDAR remote sensing of forest canopy structure and related biochemical parameters at the H.J. Andrews experimental forest, Oregon, USA. In J. D. Greer (Ed.), *Natural resources management using remote sensing and GIS* (pp. 79–91). Washington, DC: ASPRS.

Lefsky, M. A., Cohen, W. B., Parker, G. G., & Harding, D. J. (2002). LiDAR remote sensing for ecosystem studies. *Bioscience*, *52*, 19–30.

Lefsky, M. A., Harding, D., Cohen, W. B., Parker, G., & Shugart, H. H. (1999b). Surface LiDAR remote sensing of basal area and biomass in deciduous forests of eastern Maryland, USA. *Remote Sensing of Environment*, *67*, 83–98.

Lim, K., Treitz, P., Wulder, M., St-Onge, B., & Flood, M. (2003). LiDAR remote sensing of forest structure. *Progress in Physical Geography*, *27*, 88–106.

Magnussen, S., & Boudewyn, P. (1998). Derivations of stand heights from airborne laser scanner data with canopy-based quantile estimators. *Canadian Journal of Forest Research-Revue Canadienne de Recherche Forestière*, *28*, 1016–1031.

Magnussen, S., Eggermont, P., & LaRiccia, V. N. (1999). Recovering tree heights from airborne laser scanner data. *Forest Science*, *45*, 407–422.

Matthews, G. (1993). The carbon content of trees. *Forestry Commission Technical Paper*, *vol. 4*. London: Forestry Commission, HSMO.

Means, J. E., Acker, S. A., Fitt, B. J., Renslow, M., Emerson, L., & Hendrix, C. J. (2000). Predicting forest stand characteristics with airborne scanning LiDAR. *Photogrammetric Engineering and Remote Sensing*, *66*, 1367–1371.

Means, J. E., Acker, S. A., Harding, D. J., Blair, J. B., Lefsky, M. A., Cohen, W. B., et al. (1999). Use of large-footprint scanning airborne LiDAR to estimate forest stand characteristics in the Western Cascades of Oregon. *Remote Sensing of Environment*, *67*, 298–308.

Milne, R., Brown, A. W., & Murray, T. D. (1998). The effect of geographical variation of planting rate on the uptake of carbon by new forests of Great Britain. *Forestry*, *71*, 297–309.

Naesset, E. (1997a). Determination of mean tree height of forest stands using airborne laser scanner data. *ISPRS Journal of Photogrammetry and Remote Sensing*, *52*, 49–56.

Naesset, E. (1997b). Estimating timber volume of forest stands using airborne laser scanner data. *Remote Sensing of Environment*, *61*, 246–253.

Naesset, E. (2002). Predicting forest stand characteristics with airborne scanning laser using a practical two-stage procedure and field data. *Remote Sensing of Environment*, *80*, 88–99.

Naesset, E., & Okland, T. (2002). Estimating tree height and tree crown properties using airborne scanning laser in a boreal nature reserve. *Remote Sensing of Environment*, *79*, 105–115.

Nelson, R., Krabill, W., & Tonelli, J. (1988). Estimating forest biomass and volume using airborne laser data. *Remote Sensing of Environment*, *24*, 247–267.

Nelson, R., Valenti, M. A., Short, A., & Keller, C. (2003). A multiple resource inventory of Delaware using airborne laser data. *Bioscience*, *53*, 981–992.

Nilsson, M. (1996). Estimation of tree heights and stand volume using an airborne LiDAR system. *Remote Sensing of Environment*, *56*, 1–7.

Omasa, K., Qiu, G. Y., Watanuki, K., Yoshimi, K., & Akiyama, Y. (2003). Accurate estimation of forest carbon stocks by 3-D remote sensing of individual trees. *Environmental Science and Technology*, *37*, 1198–1201.

Patenaude, G. L., Briggs, B. D. J., Milne, R., Rowland, C. S., Dawson, T. P., & Pryor, S. N. (2003). The carbon pool in a British semi-natural woodland. *Forestry*, *76*, 109–119.

Ranson, K. J., Saatchi, S., & Sun, G. Q. (1995). Boreal forest ecosystem characterization with Sir-C/X Sar. *IEEE Transactions on Geoscience and Remote Sensing*, *33*, 867–876.

Rayner, P. J., Enting, I. G., Francey, R. J., & Langenfelds, R. (1999). Reconstructing the recent carbon cycle from atmospheric CO_2, delta C-13 and O-2/N-2 observations. *Tellus Series B-Chemical and Physical Meteorology*, *51*, 213–232.

Ripple, W. J., Wang, S., Isaacson, D. L., & Paine, D. P. (1991). A preliminary comparison of Landsat Thematic Mapper and Spot-1 HRV multispectral data for estimating coniferous forest volume. *International Journal of Remote Sensing*, *12*, 1971–1977.

Ruppert, G. S., Wimmer, A., Beichel, R., & Ziegel, M. (2000). Adaptive multiresolution algorithm for high precision forest floor DTM generation. In U. N. Kamerman, T. P. Singh, C. Werner, & V. V. Molebny (Eds.), *Laser radar technology and applications V. Proceedings of SPIE*, (pp. 97–105).

Salway, A. G., Murrells, T. P., Milne, R., & Ellis, S. (2001). *UK Greenhouse Gas Inventory. 1990 to 1999 Annual Report for submission under Framework Convention on Climate Change*. National Environmental Technology Centre, AEA Technology Centre.

Satchell, J. E. (1971). Feasibility study of an energy budget for Meathop Wood. In P. Duvigneaud (Ed.), *Productivity of forest ecosystems* (pp. 619–630). Paris, Spain: UNESCO.

Snedecor, G. W., & Cochran, W. G. (1980). *Statistical methods* (pp. 507). Ames, Iowa: The Iowa State University Press.

Steele, R. C., & Welch, R. C. (Eds.). (1973). *Monks wood: A nature reserve record* (p. 337). Cambridge, UK: The Nature Conservancy.

UNFCCC. (1997). Kyoto Protocol to the United Nation Framework Convention on Climate Change. http://unfccc.int/

Vogt, K. (1991). Carbon budgets of temperate forest ecosystems. *Tree Physiology*, *9*, 69–86.

Wehr, A., & Lohr, U. (1999). Airborne laser scanning—an introduction and overview. *ISPRS Journal of Photogrammetry and Remote Sensing*, *54*, 68–82.